

SUPPORTING INFORMATION

Vinylene carbonate reactivity at lithium metal surface: first-principles insights on the early steps of SEI formation

Francesca Fasulo,¹ Ana B. Muñoz-García,² Arianna Massaro,¹ Orlando Crescenzi,¹ Chen Huang,³ and Michele Pavone^{1,*}

¹*Department of Chemical Sciences, University of Naples Federico II, Napoli, Italy*

²*Department of Physics “Ettore Pancini”, University of Naples Federico II, Napoli, Italy*

³*Department of Scientific Computing, Florida State University, Tallahassee, Florida, USA*

* **Corresponding author:** michele.pavone@unina.it

Structural model for Li(001) surface

We cleave up Lithium metal bulk structure to obtain a 4x4 4L-slab model for the Li(001) surface (see Fig. S1). The number of layers has been selected by a convergence test on surface energy as function of thickness. The surface energy, γ , can be calculated as:

$$\gamma = \frac{E_{slab} - NE_{bulk}}{2A} \quad (S1)$$

where A is the area exposed by the surface, E_{slab} and E_{bulk} are the total energies of the surface slab and the Li bulk, respectively, and N is the number of formula units contained in the surface slab. The corresponding results are collected in Fig. S1.

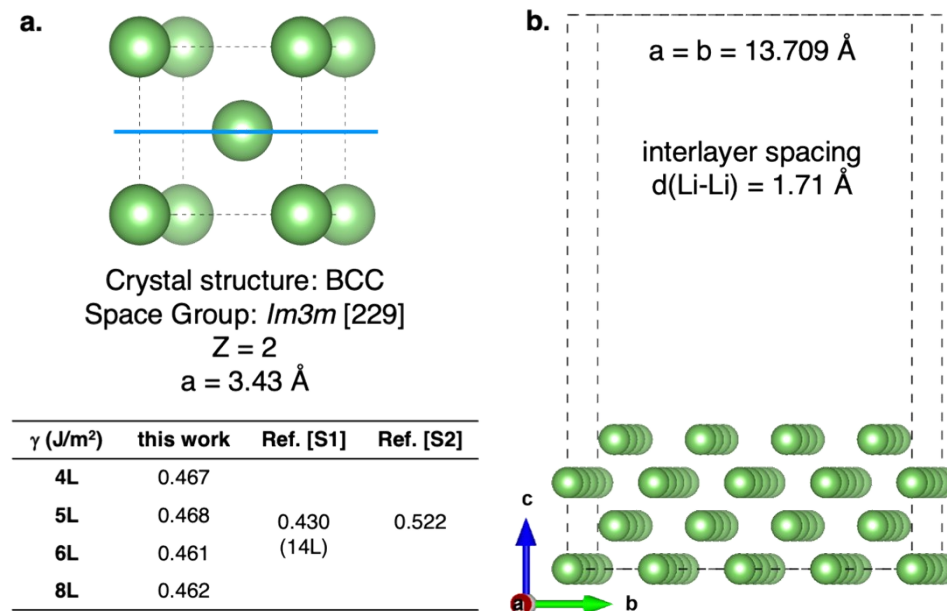
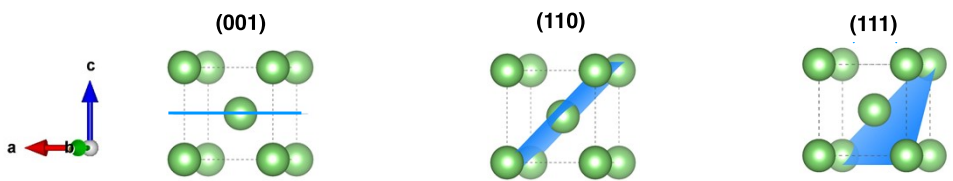


Figure S1. (a) Li bulk structure and convergence test on surface energy (γ) for the (001) termination. (b) Structural model of Li (001) 4x4 4L-slab.

The (001) lattice termination represents the most stable surface among the popular low-index orientations for Li metal: (001), (110), and (111). As shown in the following Table, the surface energies (γ , calculated according to Eq. S1) exhibit the trend: (001) < (110) < (111). The higher stability would

suggest that the (001) surface is predominant in real samples, as Li metal will preferentially expose the termination requiring minor energy expenditure.

Table S1. Surface energies calculated for (001), (110) and (111) lattice orientations of Li metal at the PBE level of theory. Structural details are displayed in the top panel. Comparison with experimental data is also reported.



		a(Å)	b(Å)	γ (J/m ²)	γ (J/m ²)
(001)	4L - 4 f.u.	3.43	3.43	0.47	0.54 [1], 0.43 [2]
(110)	4L - 8 f.u.	3.43	4.85	0.50	0.58 [1], 0.48 [2]
(111)	4L - 8 f.u.	4.85	8.39	0.52	0.60 [1], 0.55 [2]

[1] J. Wang, S.-Q. Wang. Surface Science 2014, 630, 216–224.

[2] M. Ebadi, D. Brandell, C. M. Araujo. J. Chem. Phys. 2016, 145, 204701.

Convergence tests for kinetic energy cutoff

We perform a convergence test on kinetic energy cutoff (ECUT) used in ABINIT with norm-conserving pseudo-potentials, by considering the convergence on energy and structural parameters of VC molecule. As showed in Fig. S2, the ECUT converges at 1000 eV. The structural parameters are also in good agreement with experimental values (see Ref. [S3]).

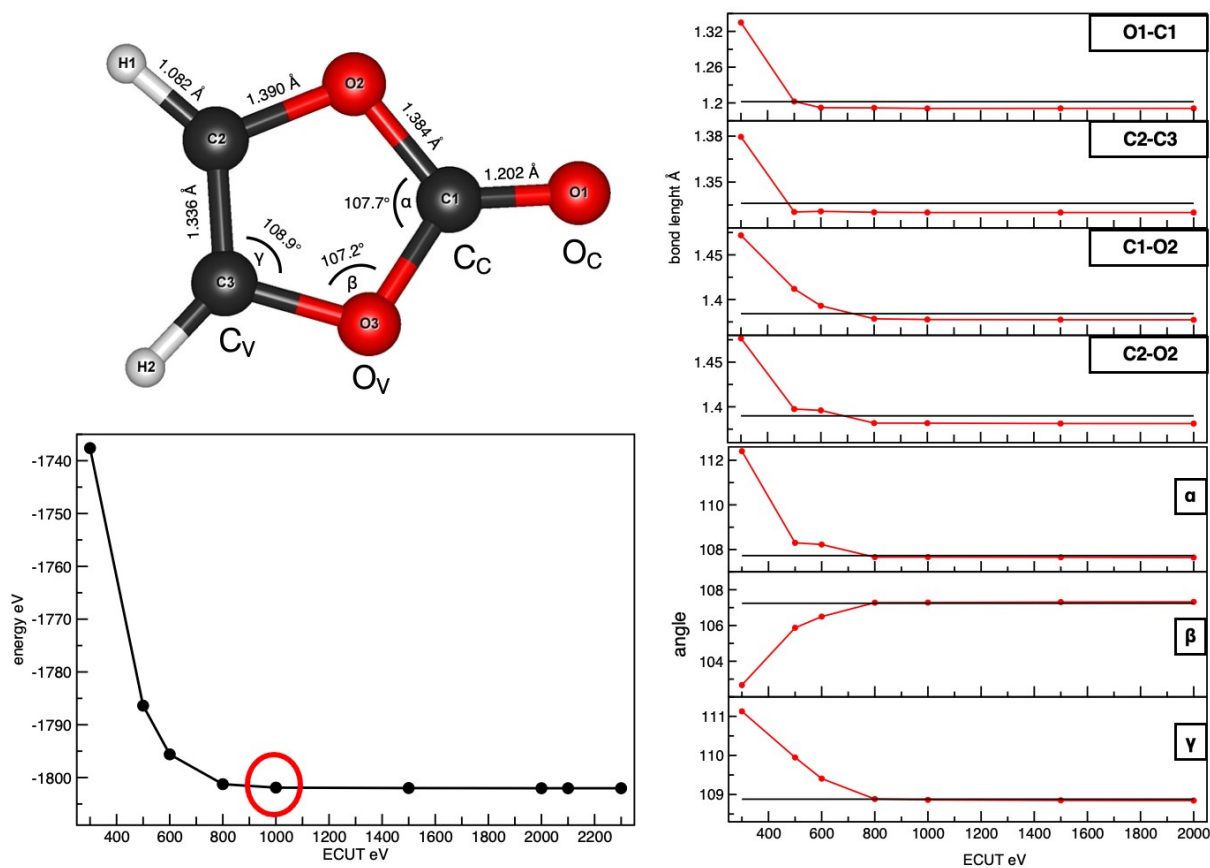


Figure S2. (top-left) Minimum-energy structure of VC molecule obtained with VASP-based methods at the PBE-D3 level of theory; Convergence tests of kinetic energy cutoff on the VC total energy (bottom-left) and structural parameters (right panels) performed with ABINIT code (the black horizontal line indicates the experimental values from Ref. [S3]). Color code: O (red), C (black), H (white), ABINIT-derived values (red lines), VASP-derived values (black lines).

VC adsorption: structural analysis

Fig. S3 shows the minimum-energy structures resulting from geometry optimization at PBE-D3 level of theory. We can see that the parallel adsorption is not stable, and the VC molecule rearranges in bridged (b) and end-on (e) configurations by tilting (t) with respect to the surface.

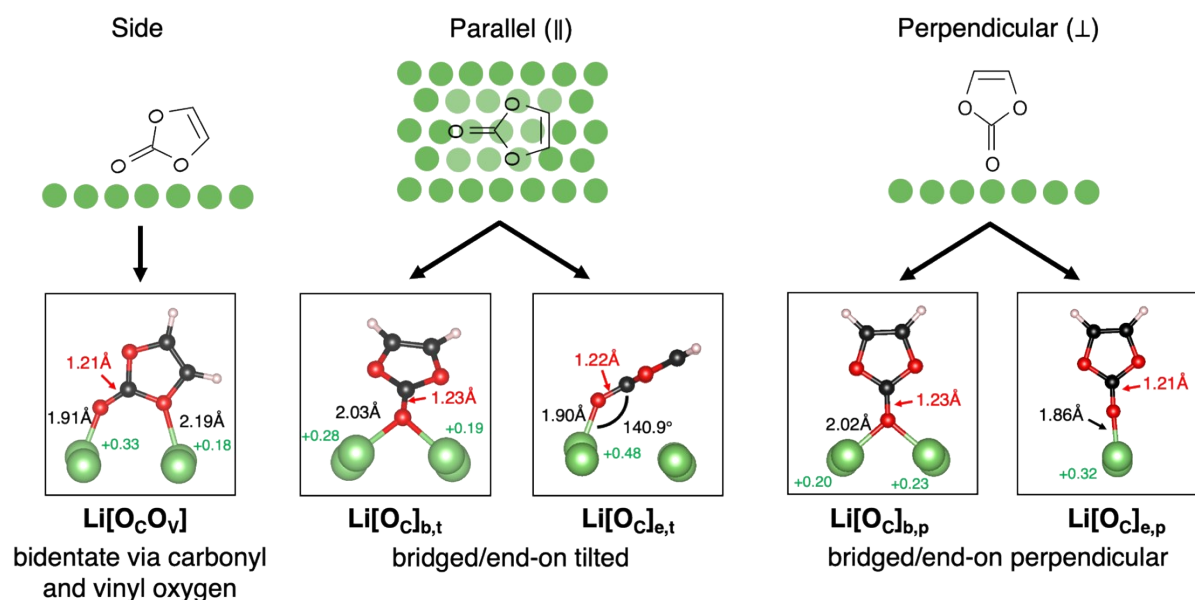


Figure S3. Representation scheme for the considered adsorption modes: (from left to right) bidentate, monodentate-parallel, and monodentate-perpendicular, leading to $\text{Li}[\text{O}_C\text{O}_V]$, $\text{Li}[\text{O}_C]_{b,t}$ and $\text{Li}[\text{O}_C]_{e,t}$, $\text{Li}[\text{O}_C]_{b,p}$ and $\text{Li}[\text{O}_C]_{e,p}$ respectively. Relevant structural parameters and electronic charges are displayed. Color code as in Fig. 1.

The dihedral ($\text{O}_V, \text{O}_V\text{-C}=\text{O}$) angle for the VC molecule in the considered adsorption modes are reported in Table S2. Dihedral angle of 180° represents a planar geometry, while values $< 180^\circ$ indicate a certain pyramidalization at the C_C atom.

Table S2. The dihedral ($\text{O}_V, \text{O}_V\text{-C}=\text{O}$) angle for the VC molecule in each adsorption mode.

	$\text{Li}[\text{O}_C\text{O}_V]$	$\text{Li}[\text{O}_C]_{b,t}$	$\text{Li}[\text{O}_C]_{b,p}$	$\text{Li}[\text{O}_C]_{e,t}$	$\text{Li}[\text{O}_C]_{e,p}$
Dihedral ($\text{O}_V, \text{O}_V\text{-C}=\text{O}$)	179.60°	174.67°	179.37°	179.64°	179.97°

Fig. S4 shows the projected Density of States (pDOS) of the unbound state Li+VC and isolated VC molecular system (i.e., inside a 10 Å-cubic cell to avoid intermolecular interactions). We can see that Li surface has no effect on electronic structure of VC placed at ~ 5 Å.

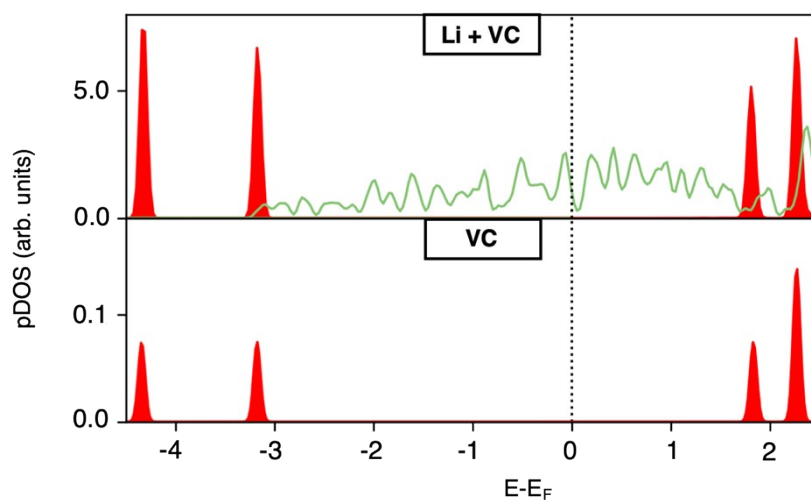


Figure S4. Projected Density of States (pDOS) of the Li+VC unbound state (separated by ~ 5 Å distance) and isolated VC molecular system (i.e., inside a 10 Å-cubic cell to avoid intermolecular interactions). Due to different choice of Fermi energies in the two cases, the energies of isolated VC are shifted respect to Li+VC system. Color code as in Fig. 2.

VC dissociation: structural and electronic analysis on DISS(C_CO_V) and DISS(C_VO_V) states

Fig. S5 shows the structural analysis (bond lengths and Li atoms displacement along z axis), the Bader charge variation, the charge density different plots of the two dissociated states, DISS(C_CO_V) and DISS(C_VO_V).

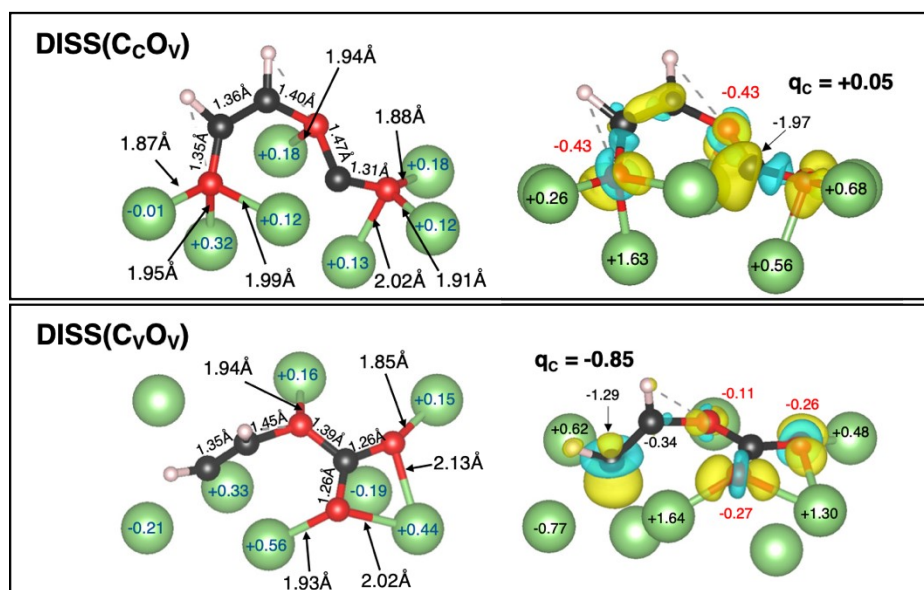


Figure S5. Structural details of the first reaction intermediates, $DISS(C_C O_V)$ and $DISS(C_V O_V)$, Bader charge variation on Li (in black) and O (in red) atoms, Δq (calculated according to Eq. 3), and corresponding charge density difference plots (isosurface $1 \text{ meV}/\text{\AA}^3$). The net charge on C_C and C_V carbon atoms is displayed in bold. Color code as in Fig. 1.

VC-Li interaction by DFET: method validation

We provide a high-level description of the VC ring-opening processes on Li metal surface with the Density Functional Embedding Theory (DFET). The embedding potential (V_{emb}) is solved for two clusters of different size, as showed in Fig. S6a. Both clusters are cut from the 4×4 supercell of (001)-Li surface, so that we have:

- a small cluster, containing 8 Li atoms (*i.e.*, 8-Li), and an environment of 56 Li atoms,
- a larger cluster, with 12 Li atoms (*i.e.*, 12-Li), and an environment of 52 Li atoms.

To validate our method, both the embedded subsystem and the background region are described at the DFT level with PBE functional (PBE-in-PBE). If the embedding potential was exact, a DFT treatment of both regions should produce the same cluster electron density as from a periodic DFT calculation on

the total system. In this way, we can directly compare the cluster electron density obtained at PBE-in-PBE embedding calculations with the previously reported PBC analysis. Fig. S6b shows the electron densities within embedded region projected on the b axis for the periodic system (black line), the 8-Li (red line) and 12-Li (orange line) clusters. There is a good agreement among the three projected electron densities within the explored b-axis range. It seems that the accuracy is not improving sensibly with the cluster size, as the average variation from the periodic density is of $4 \times 10^{-4} \text{ e}/\text{\AA}^3$ and $3 \times 10^{-4} \text{ e}/\text{\AA}^3$ for the 8- and 12-Li clusters, respectively. Then, we use the so-obtained V_{emb} to perform DFET calculations on the two most favorite adsorption configurations, $\text{Li}[\text{O}_\text{C}\text{O}_\text{V}]$, $\text{Li}[\text{O}_\text{C}]_{\text{b,t}}$, and the two open-VC dissociated states, $\text{DISS}(\text{C}_\text{C}\text{O}_\text{V})$ and $\text{DISS}(\text{C}_\text{V}\text{O}_\text{V})$. Again, the projected electron densities of periodic systems and the clusters are compared (see Fig. S6c). In this case, we also solve the V_{emb} for the four VC_8-Li clusters and compare the projected electron densities with the other ones (green line in Fig. 6c). This latter case gives the best agreement with periodic densities (see comparison with black lines in the plot). As the calculation of specific V_{emb} for each system would significantly increase the computational cost, we select the V_{emb} from the 12-Li cluster as the best choice for our investigation, showing a negligible variation of $5 \times 10^{-4} \text{ e}/\text{\AA}^3$ from the periodic PBE density for all the explored states.

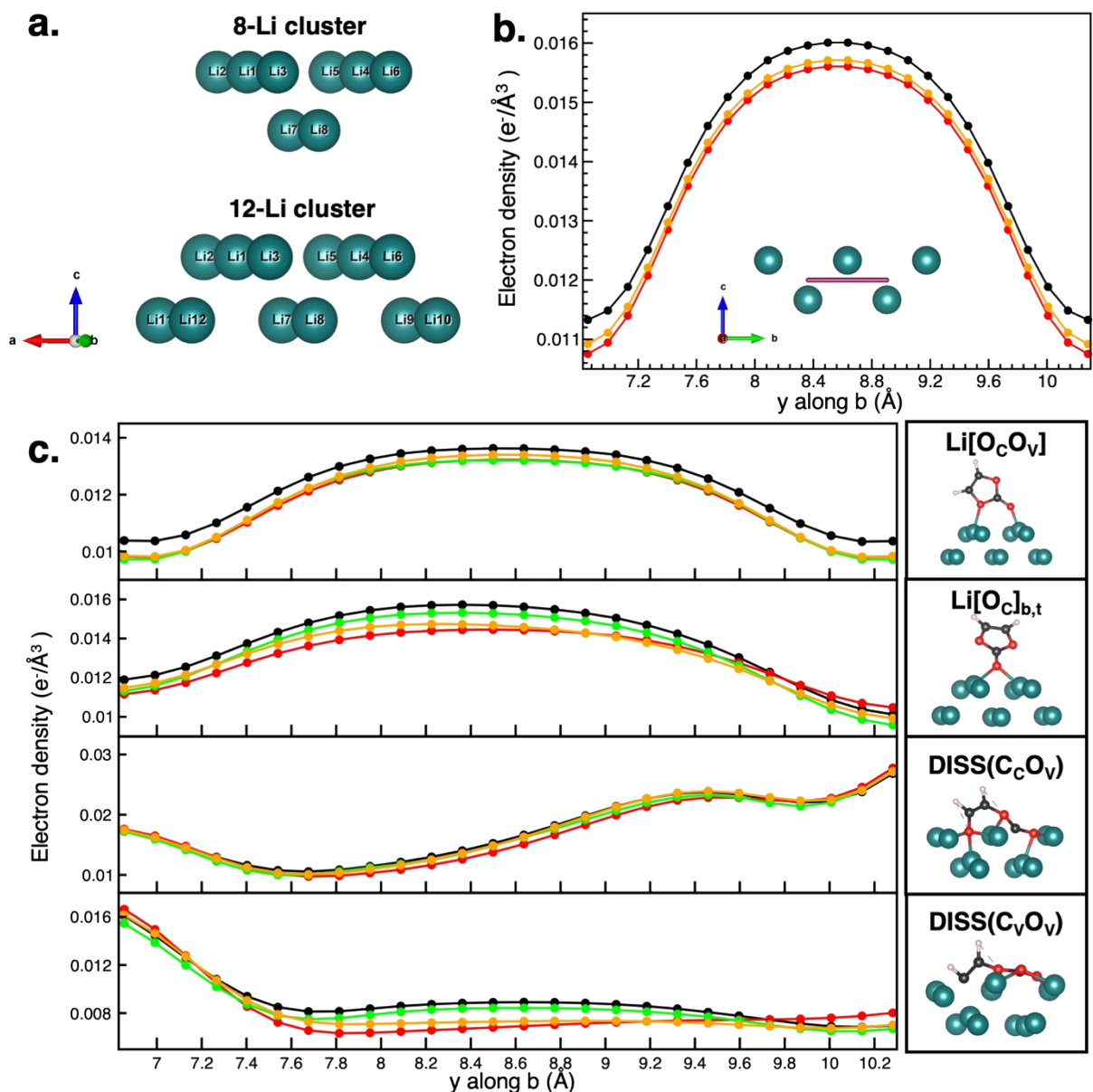


Figure S6. (a) Different-sized clusters for Li surface, containing 8 and 12 Li atoms; (b) Plot of electron densities projected on b axis for Li surface: periodic DFT-PBE (black), 8-Li cluster DFET-PBE-in-PBE (red) and 12-Li cluster DFET-PBE-in-PBE (orange); (c) Plot of electron densities projected on b axis for VC adsorbed/dissociated states on Li surface: black line refers to periodic DFT-PBE model, red and orange ones refer to, respectively, 8-Li and 12-Li using V_{emb} solved for corresponding clusters, green line refers to obtained with V_{emb} solved for each VC adsorbed/dissociated state on 8-Li.

To unveil the accuracy of DFET method in describing the VC/Li interface, we evaluate the relative energies of DISS(C_CO_V) and DISS(C_VO_V) with respect to Li[O_C]_{b,t} as:

$$\Delta E = E_{DISS(C_C O_V)/DISS(C_V O_V)} - E_{Li[O_C]_{b,t}} \quad (S2)$$

And the adsorption/dissociation energies of the two adsorbed/dissociated states (Li[O_CO_V], Li[O_C]_{b,t} / DISS(C_CO_V) and DISS(C_VO_V)) with respect to the unbound state, E_(Li+VC), as follows:

$$E_{ads/dis} = E_{ads/diss - VC@Li} - E_{(Li + VC)} \quad (S3)$$

Both these quantities are calculated from periodic models at DFT-PBE level of theory using PAW and NC pseudopotentials, and from embedded cluster models at DFET-PBE level of theory ($E_{Li-VC,cluster}^{PBE}[V_{emb}]$) by using the embedding potential solved for 8-Li, 12-Li and VC_8-Li. The resulting values are plotted in Fig. S7. Also in this case, the V_{emb} solved for the 12-Li clusters gives the best agreement with DFT-PBE results (see comparison with black/magenta and orange lines in the plot). Thus, the 12-Li cluster and the corresponding V_{emb} at PBE level of theory represents the best choice for further DFET investigation on VC/Li interface thanks to the suitable description of the VC adsorbed/dissociated states on Li surface.

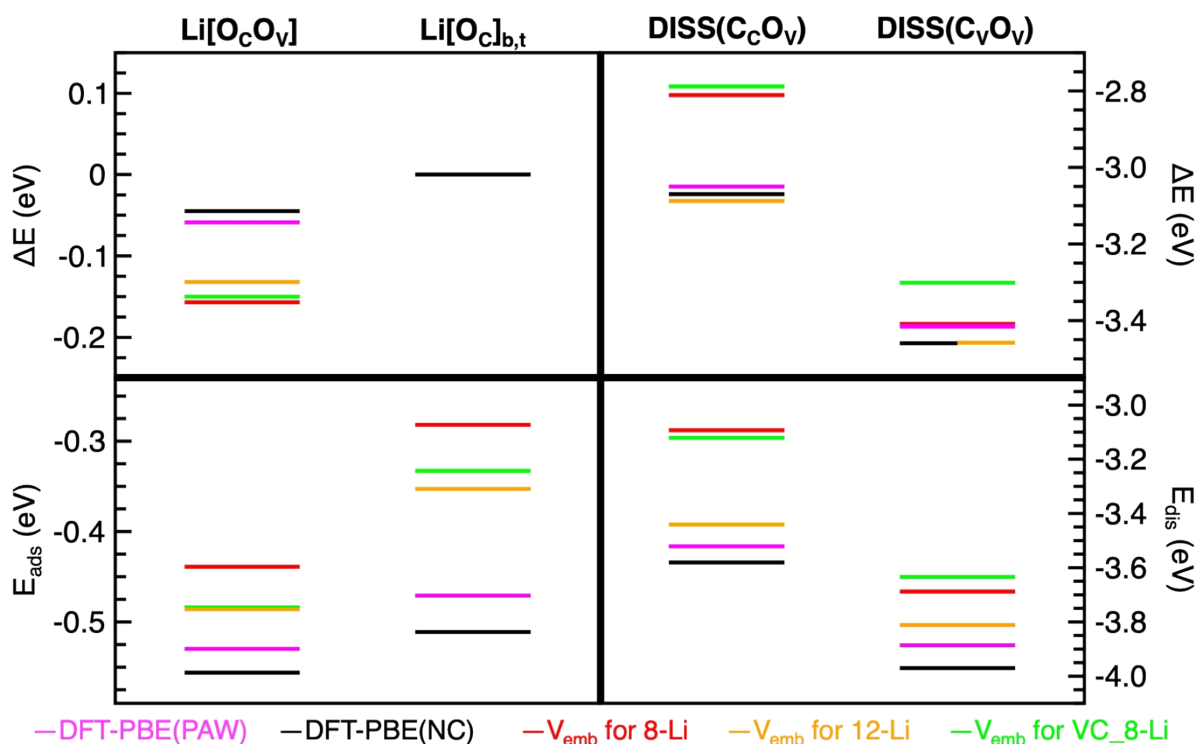


Figure S7. Relative energies (**top**) and adsorption/dissociation energies (**bottom**) calculated according to Equation S2 and S3 from DFT-PBE(PAW) (magenta), DFT-PBE(NC) (black), 8-Li (red), 12-Li (orange) and VC_8-Li (green) V_{emb} DFET-PBE-in-PBE methods.

VC ring-opening reaction mechanisms: structural and electronic analysis along MEPs

The values of energy barrier (E_1-E_0) at DFT-PBE(PAW), DFT-PBE(NC) and DFET-HSE06-in-PBE are reported in Table S3.

Table S3. The energy barrier (E_1-E_0) at DFT-PBE(PAW), DFT-PBE(NC) and DFET-HSE06-in-PBE.

E_1-E_0 (eV)	DFT-PBE(PAW)	DFT-PBE(NC)	DFET-HSE06-in-PBE
DISS(C_cO_v)	9.0E-03	0.12	0.34
DISS(C_vO_v)	2.4E-04	0.10	0.29

In Fig. S8, Bader charges (q_M) on C_C and O_V atoms in $DISS(C_C O_V)$ and C_V and O_V in $DISS(C_V O_V)$ are plotted for each intermediate along the MEPs obtained from NEB calculations. There is an overall charge decrease for all the atoms involved in the bond-breaking. In particular, the significant lowering of C_C and C_V net charges (black lines in Fig. S7) clearly suggest that a reductive mechanism is taking place, as a result of the before-mentioned charge transfer from the Li(001) surface.

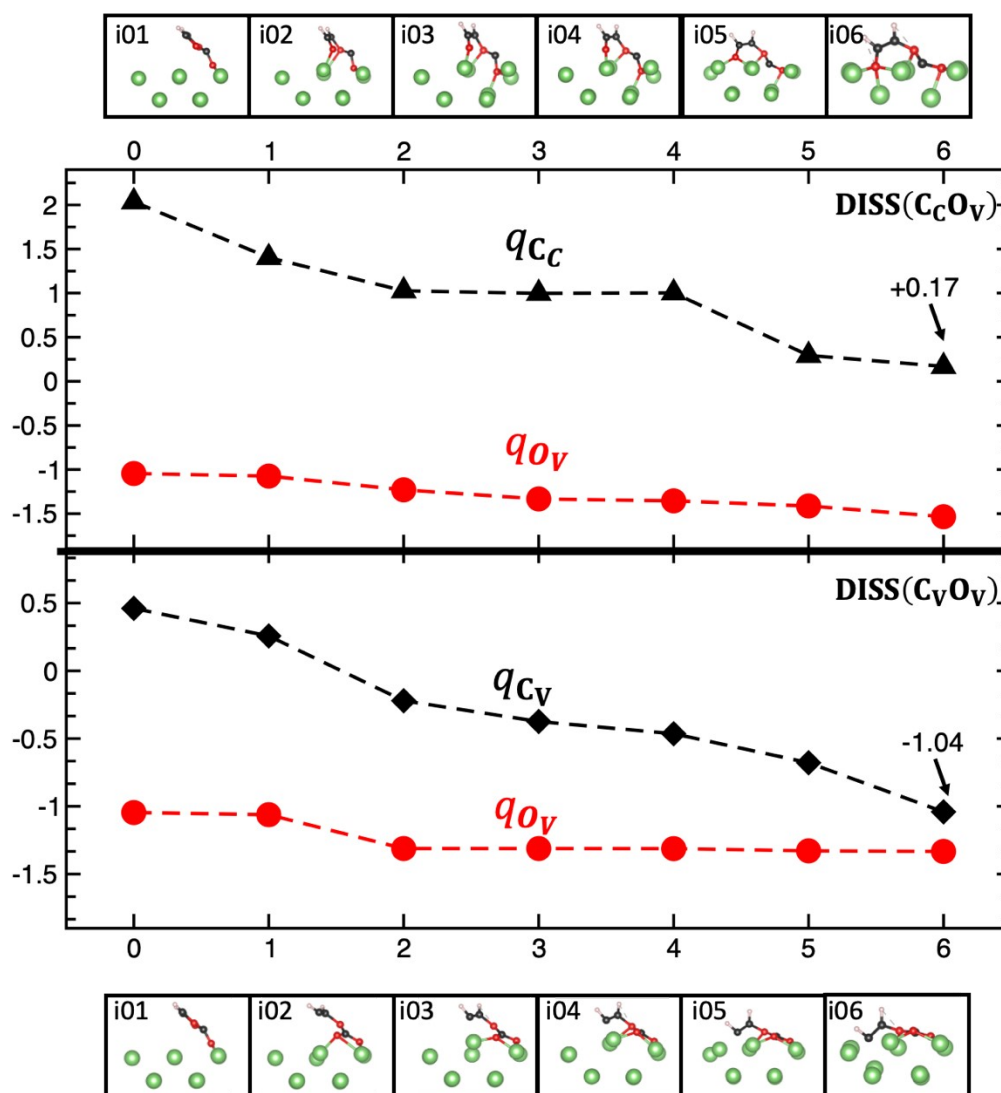


Figure S8. Bader charges on the atoms involved in the dissociation processes, $DISS(C_C O_V)$ (q_{C_C} and q_{O_V}) and $DISS(C_V O_V)$ (q_{C_V} and q_{O_V}), along the MEPs obtained from CI-NEB calculations. Colour code as in Fig. 1.

REFERENCES

[S1] M. Ebadi, D. Brandell, C. M. Araujo. “Electrolyte decomposition on Li-metal surfaces from first-principles theory”. *J. Chem. Phys.* 2016, 145, 204701.

[S2] W.R. Tyson, W.A. Miller. “Surface free energies of solid metals: Estimation from liquid surface tension measurements”. *Surf. Sci.* 1977, 62, 267.

[S3] W.F. White. “Microwave Spectra of ^{13}C - and ^{18}O -Containing Species and the Structure of Vinylene Carbonate” Boggs. *J. Chem. Phys.* 1971, 54, 4714